IEICE TRANS. ELECTRON., VOL.E99–C, NO.1 JANUARY 2016

BRIEF PAPER

Experimental Study on Embedded Object Imaging Method with Range Point Suppression of Creeping Wave for UWB Radars

Toshiki MANAKA[†], *Nonmember*, **Shouhei KIDERA**[††a)], *and* **Tetsuo KIRIMOTO**[††], *Members*

SUMMARY Ultra-wideband radar exhibits high range resolution, and excellent capability for penetrating dielectric media, especially when using lower frequency microwaves. Thus, it has a great potential for innovative non-destructive testing of aging roads or bridges or for non-invasive medical imaging applications. In this context, we have already proposed an accurate dielectric constant estimation method for a homogeneous dielectric medium, based on a geometrical optics (GO) approximation, where the dielectric boundary points and their normal vectors are directly reproduced using the range point migration (RPM) method. In addition, to compensate for the estimation error incurred by the GO approximation, a waveform compensation scheme employing the finite-difference time domain (FDTD) method was incorporated. This paper shows the experimental validation of this method, where a new approach for suppressing the creeping wave along the dielectric boundary is also introduced. The results from real observation data validate the effectiveness of the proposed method in terms of highly accurate dielectric constant estimation and embedded object boundary reconstruction.

key words: *UWB radars, range points migration (RPM), dielectric constant estimation, non-destructive testing, internal imaging*

1. Introduction

Ultra-wideband (UWB) radar, with its high range resolution and ability to penetrate a dielectric medium, is promising for various internal imaging applications. For instance, in non-destructive testing of aging walls, roads and bridges, where cavities or cracks within the concrete material need to be detected. Additionally, there are various studies on medical imaging for the early detection of breast cancer, where a distinguishable echo from a malignant tumor is used to identify its location. Various internal imaging techniques, such as the time-reversal method [1] and the space-time beamforming method [2], have been established for these applications. However, these methods are based on signal waveform integration, which often requires a large computational calculation or is not accurate enough to identify the detailed structure of a target.

For these applications, we have already proposed an accurate and fast imaging method [3] for targets embedded in a dielectric medium. This method is based on the advanced principle of the range points migration (RPM) method [4], which accurately determines the propagation path in a dielectric medium by exploiting the target boundary points and their normal vectors under a geometrical optics (GO) approximation. Although this method enhances the imaging accuracy and significantly reduces the amount of computation by specifying boundary extraction for a homogeneous medium, it also requires an accurate dielectric constant estimation method to maintain its imaging accuracy.

There are various types of permittivity estimation methods, based on an inverse scattering scheme for domain integral equations [5]. Although these methods can directly reconstruct the spatial distribution of both real and imaginary parts of the permittivity, there is a severe limitation on space discretization size to avoid sluggish convergence in higher-dimensional optimizations. Other methods such as a geometric optics approximation for through-the-wall imaging (TWI) applications [6] require less computational resource compared with those based on inverse scattering; however, there is a severe limitation in that these methods assume a known and simple shape for the dielectric medium, such as a rectangle.

As a low computational and accurate dielectric constant estimation method, we have already proposed the method by employing an outer dielectric boundary, which can be accurately reconstructed by RPM, for propagation path estimation, based on the GO approximation [7]. Furthermore, this method employs the finite difference time domain (FDTD) method to compensate for the estimation error in the GO approximation, caused by a waveform discrepancy between the transmissive and transmitted signals. However, this method suffers in some dielectric object cases, where an undesirable signal propagating along dielectric outer boundary, the so called creeping wave, is not negligible in the received signal. To overcome this difficulty, this paper introduces a new approach for suppressing a creeping wave without using *a priori* knowledge of the shape or location of the dielectric object, and show the experimental validation of this method. In the experiment, we assume a simplified non-destructive testing situation, where a metallic object is embedded in a homogeneous cement medium. The results demonstrate that the highly accurate dielectric constant estimation and the internal imaging of the order of 1/100 the transmitting center wavelength, are simultaneously achieved using the proposed method, where the creeping wave component is efficiently suppressed by the newly introduced approach.

Manuscript received July 1, 2015.
Manuscript revised September 3, 2015.

[†]The author is with Graduate School of Bioengineering, The University of Tokyo, Tokyo, 113–8654 Japan.
[††]The authors are with Graduate School of Informatics and Engineering, The University of Electro-Communications, Chofu-shi, 182–8585 Japan.
a) E-mail: kidera@ee.uec.ac.jp

DOI: 10.1587/transele.E99.C.138

Copyright © 2016 The Institute of Electronics, Information and Communication Engineers

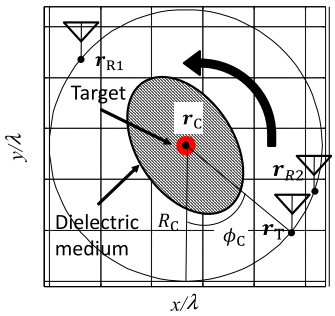

Fig. 1 System model.

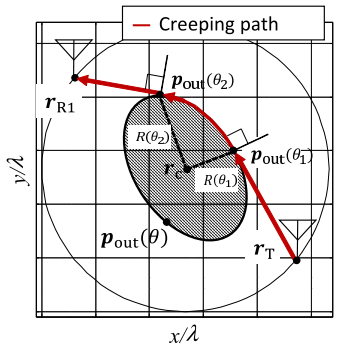

Fig. 2 Propagation path of creeping wave.

2. System Model

Figure 1 shows the system model. We assume that an inner target and surrounding outer dielectric object have unknown shapes with clear boundaries. A dielectric object is assumed to be a homogeneous, non-dispersive, and lossy medium. The center location of an antenna scanning orbit is defined as $\boldsymbol{r}_{\mathrm{C}}$. One omni-directional transmitting antenna is located at $\boldsymbol{r}_{\mathrm{T}} = (X_{\mathrm{T}}, Y_{\mathrm{T}})$. One receiving antenna is located at $\boldsymbol{r}_{\mathrm{R1}} = (X_{\mathrm{R1}}, Y_{\mathrm{R1}})$, where $\boldsymbol{r}_{\mathrm{C}} = (\boldsymbol{r}_{\mathrm{R1}} + \boldsymbol{r}_{\mathrm{T}})/2$ holds. The other receiving antenna is located at $\boldsymbol{r}_{\mathrm{R2}} = (X_{\mathrm{R2}}, Y_{\mathrm{R2}})$, which is adjacent to the transmitting antenna. These three antennas simultaneously scan along the circle with center $\boldsymbol{r}_{\mathrm{C}}$ and radius R_{C}. A mono-cycle pulse is used as the transmitting signal, the center wavelength of which is defined as λ. $S_{\mathrm{R1}}(\boldsymbol{r}_{\mathrm{R1}}; R)$ and $S_{\mathrm{R2}}(\boldsymbol{r}_{\mathrm{R2}}; R)$ are defined as the outputs of the Wiener filter at antenna positions $\boldsymbol{r}_{\mathrm{R1}}$ and $\boldsymbol{r}_{\mathrm{R2}}$, respectively, where $R = ct/2$ is a function of time t and the propagation speed of the radio wave c in the air. The range points extracted from the local maxima in S_{R1} and S_{R2} are defined as $\boldsymbol{q}_{\mathrm{R1},i} = (X_{\mathrm{R1},i}, Y_{\mathrm{R1},i}, R_{\mathrm{R1},i}), (i = 1, \ldots, N_{\mathrm{R1}})$ and $\boldsymbol{q}_{\mathrm{R2},i} = (X_{\mathrm{R2},i}, Z_{\mathrm{R2},i}, R_{\mathrm{R2},i}), (i = 1, \ldots, N_{\mathrm{R2}})$, respectively, the detailed process of which is described in [4]. From the set of $\boldsymbol{q}_{\mathrm{R2}}$, we select $\boldsymbol{q}^{\mathrm{D}}_{\mathrm{R2}}$ which has maximal amplitude of $S_{\mathrm{R2}}(\boldsymbol{q}_{\mathrm{R2}})$ at each antenna location. These are regarded as range points corresponding to the outer dielectric boundary. The set of $\boldsymbol{q}_{\mathrm{R2}}$ except for the set of $\boldsymbol{q}^{\mathrm{D}}_{\mathrm{R2}}$ are defined as the set of $\boldsymbol{q}^{\mathrm{T}}_{\mathrm{R2}}$, which are regarded as those corresponding to an inner target boundary.

3. Dielectric Constant and Internal Shape Estimation

We have already proposed the promising method [7], which accomplishes highly accurate dielectric constant estimation and embedded object imaging by combining with the FDTD method (once only) to compensate for the estimation errors caused by the GO approximation. However, this method suffers from degrading accuracy when a creeping wave, propagating along the dielectric outer boundary, is not negligible in the received signal on the location $\boldsymbol{r}_{\mathrm{R1}}$. To overcome this problem, this paper proposes a method for eliminating range points caused by creeping waves without using *a priori* information of the shape and location of the dielectric object. In the following subsections, the methodology to suppress the creeping wave is first explained, and the existing dielectric constant estimation method [7] is briefly introduced for reference.

3.1 Suppression of Range Points Caused by Creeping Wave

To establish the elimination of the range points caused by a creeping wave, first, this method obtains the outer dielectric boundary points and their normal vectors by applying the RPM method to the range points, $\boldsymbol{q}^{\mathrm{D}}_{\mathrm{R2}}$. In addition, to obtain target points and normal vectors on the dielectric boundary with a sufficiently dense interval, the Envelope interpolation described in [8] is also introduced. Especially, the Envelope method can express a dielectric outer boundary with parameter θ, $(0 \le \theta \le 2\pi)$ as $\boldsymbol{p}_{\mathrm{out}}(\theta) = \boldsymbol{r}_c + R(\theta)(\cos\theta, \sin\theta)$. In most cases, the creeping wave, propagating along the outer dielectric boundary is included in the received signal $S_{\mathrm{R1}}(\boldsymbol{q}_{\mathrm{R1}})$. To identify the transmissive delay penetrating the dielectric object, the range points corresponding to the creeping wave need to be suppressed. For this suppression, the propagation distance of the creeping wave from $\boldsymbol{r}_{\mathrm{T}}$ to $\boldsymbol{r}_{\mathrm{R1}}$ as $R_{\mathrm{creep}}(\boldsymbol{r}_{\mathrm{T}}, \boldsymbol{r}_{\mathrm{R1}})$ is calculated:

$$R_{\mathrm{creep}}(\boldsymbol{r}_{\mathrm{T}}, \boldsymbol{r}_{\mathrm{R1}}) = \int_{\theta_1}^{\theta_2} R(\theta)\mathrm{d}\theta + \|\boldsymbol{r}_{\mathrm{T}} - \boldsymbol{p}_{\mathrm{out}}(\theta_1)\| + \|\boldsymbol{r}_{\mathrm{R1}} - \boldsymbol{p}^{\mathrm{out}}(\theta_2)\|, \quad (1)$$

$\boldsymbol{p}_{\mathrm{out}}(\theta_1)$ and $\boldsymbol{p}_{\mathrm{out}}(\theta_2)$ are the incident and emission points on the dielectric boundary for the creeping wave, which is determined by the condition that their normal vectors are perpendicular to the radial direction from the transmitting and receiving antennas. In this case, the range points $\boldsymbol{q}_{\mathrm{R1}} = (X_{\mathrm{R1}}, Z_{\mathrm{R1}}, R_{\mathrm{R1}})$ satisfying $|R_{\mathrm{R1}} - R_{\mathrm{creep}}(\boldsymbol{r}_{\mathrm{T}}, \boldsymbol{r}_{\mathrm{R1}})| < \delta$ are eliminated, where δ is empirically determined. It should be noted that there is the limitation for this suppression, in the case that the difference between the creeping and penetrating paths becomes smaller than the range resolution, namely pulse width. The remaining range points are defined as $\tilde{\boldsymbol{q}}_{\mathrm{R1}} = (\tilde{X}_{\mathrm{R1}}, \tilde{Z}_{\mathrm{R1}}, \tilde{R}_{\mathrm{R1}})$, and regarded as the range points corresponding to the transmissive signal. Figure 2 shows estimation example of propagation path for the creeping wave.

3.2 Combination with Dielectric Constant Estimation

The existing dielectric constant estimation method [7] is briefly explained for reference purposes. To estimate the dielectric constant of a surrounding outer medium, this method calculates the dielectric constant by minimizing the difference between an observed and estimated propagation delay as:

$$\epsilon_{\mathrm{t}}^{\mathrm{init}}\left(\tilde{\boldsymbol{q}}_{\mathrm{R1},i}\right) = \arg\min_{\epsilon_{\mathrm{t}}} \left| R\left(\epsilon_{\mathrm{t}}; \tilde{X}_{\mathrm{R1},i}, \tilde{Y}_{\mathrm{R1},i}\right) - \tilde{R}_{\mathrm{R1},i} \right|^2, \quad (2)$$

where $R(\epsilon_t; \tilde{X}_{\mathrm{R1},i}, \tilde{Y}_{\mathrm{R1},i})$ is the estimated propagation delay using the Envelope boundary points expressed as $\boldsymbol{p}_{\mathrm{out}}(\theta)$ and their normal vectors determined by the GO approximation detailed in [7]. Using all transmissive range points, the initial dielectric constant $\epsilon_t^{\mathrm{init}}$ is estimated as:

$$\hat{\epsilon}_{\mathrm{t}}^{\mathrm{init}} = \frac{\sum_{\tilde{\boldsymbol{q}}_{\mathrm{R1},i}\in Q} S_{\mathrm{R1}}\left(\tilde{\boldsymbol{q}}_{\mathrm{R1},i}\right) \epsilon_{\mathrm{t}}^{\mathrm{init}}\left(\tilde{\boldsymbol{q}}_{\mathrm{R1},i}\right)}{\sum_{\tilde{\boldsymbol{q}}_{\mathrm{R1},i}\in Q} S_{\mathrm{R1}}\left(\tilde{\boldsymbol{q}}_{\mathrm{R1},i}\right)}, \quad (3)$$

where $Q = \left\{ \tilde{\boldsymbol{q}}_{\mathrm{R1},i} \middle| \left| \epsilon_t\left(\tilde{\boldsymbol{q}}_{R1,i}\right) - \tilde{\epsilon}_t \right| < \Delta\epsilon_t \right\}$, where $\tilde{\epsilon}_t$ is the mode value in $\epsilon_t\left(\tilde{\boldsymbol{q}}_{\mathrm{R1},i}\right)$ and $\Delta\epsilon_t$ is the threshold to eliminate outliers. Furthermore, to reduce the estimation error caused by waveform mismatch between the transmitted and transmissive waves, the compensation scheme based on FDTD signal regeneration is applied [7]. The details on this approach are described in [7]. The final dielectric constant $\hat{\epsilon}_{\mathrm{t}}$ is determined in similar to Eq. (3). Lastly, the boundary of the embedded target is estimated by the extended RPM method described in [3], employing $\hat{\epsilon}_{\mathrm{t}}$ and $\boldsymbol{q}_{\mathrm{R2}}^{\mathrm{T}}$.

4. Performance Evaluation in Experiment

This section describes the experimental validation of the method previously mentioned. The upper side of Fig. 3 illustrates the experimental setup. To guarantee a sufficient accuracy for target manufacturing, this experiment assumes a simple shape case, where the cylindrical aluminum (internal object) is embedded in the cylindrical cement (dielectric object), and they are both 250 mm high. The radii of the cement and aluminum objects are 139 mm and 25 mm, respectively. The circular scanning model described in Sect. 2 is equivalently accomplished by rotating the dielectric object along the center $\boldsymbol{r}_{\mathrm{C}}$, fixing the location of the antennas $\boldsymbol{r}_{\mathrm{T}}$, $\boldsymbol{r}_{\mathrm{R1}}$ and $\boldsymbol{r}_{\mathrm{R2}}$. The target rotation center is set to $\boldsymbol{r}_{\mathrm{C}} = (400\mathrm{mm}, 400\mathrm{mm})$, and the distance from the antenna, namely, R_{C} is set to 400 mm. The received signal is obtained using a VNA (Vector Network Analyzer), where the frequency is swept from 1000 MHz to 3000 MHz at 10 MHz intervals. The effective bandwidth is around 2.0 GHz, namely, the range resolution is around 75 mm. The center frequency is also 2.0 GHz (center wavelength: 150 mm). The actual dielectric constant of the dielectric object (cement) is measured as 9.07 by assessing the propagation delay when observing a cement object with a cuboid shape as shown in the lower side of Fig. 3.

Figure 4 illustrates the outputs of the Wiener filter at $S_{\mathrm{R1}}(\boldsymbol{r}_{\mathrm{R1}}; R)$ for each rotation angle ϕ_{C} before and after applying the creeping signal suppression method described in Sect. 3.1, respectively. The left side of Fig. 4 shows that each receiving antenna located at $\boldsymbol{r}_{\mathrm{R1}}$ receives a strong signal propagating around the dielectric outer boundary, namely, the creeping wave, the range points extracted from which need to be eliminated for the dielectric constant estimation of the dielectric object. Note that, while there must be a whispering-gallery mode wave propagating into dielectric medium [9], such wave propagates into dielectric medium, and its propagation velocity become considerably slower than that of creeping wave. The right side of Fig. 4 verifies that the proposed approach for suppressing creeping wave successfully extracts only range points, which corresponds to a transmissive signal penetrating into dielectric object. The average SNR for reflection signals from outer and inner boundaries received at $\boldsymbol{r}_{\mathrm{R2}}$ are 51 dB and 35 dB, respectively. Also, the average SNR for transmissive signals received at $\boldsymbol{r}_{\mathrm{R1}}$ is 43 dB. Figure 5 shows the histograms of the estimated dielectric constant for all the range points of $\tilde{\boldsymbol{q}}_{\mathrm{R1}}$, before and after the compensation using the FDTD data reproduction. Note that the FDTD data regeneration is carried out only once, and it is sufficient to compensate for the

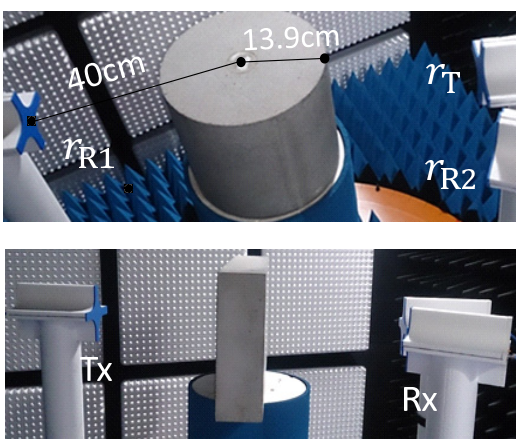

Fig. 3 Setup for the experiment (upper) and setup for obtaining actual dielectric constant of cement object (lower).

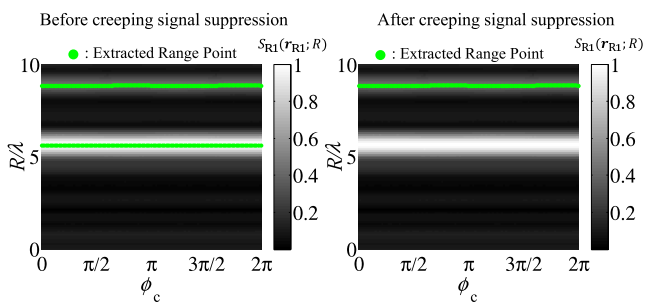

Fig. 4 Outputs of Wiener filter as $S_{\mathrm{R1}}(\boldsymbol{r}_{\mathrm{R1}}; R)$ and extracted range points before (left) and after (right) creeping wave suppression.

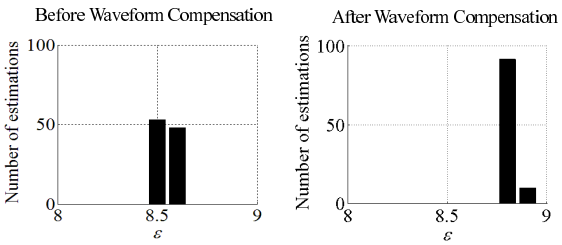

Fig. 5 Histogram of dielectric constant estimation before (left) and after (right) waveform compensation by FDTD method.

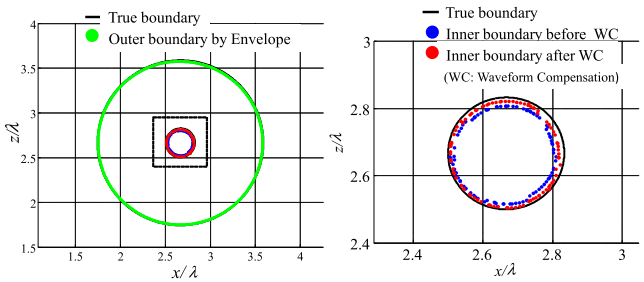

Fig. 6 Actual and reconstructed image before and after waveform compensation (WC) (right: enlarged view for internal object).

range estimation error caused by the waveform discrepancy. The reason for this fact is more detailed in [7]. This figure verifies that the FDTD-based waveform compensation significantly enhances the accuracy of the dielectric constant estimation. The weighted average dielectric constants before and after waveform compensation are 8.52 and 8.80, and the relative errors are 6% and 3% respectively. This shows that the proposed method accomplishes highly accurate dielectric constant estimation without knowledge of the shape of the dielectric media using real data. Furthermore, the right side and left side of Fig. 6 illustrate the actual and estimated dielectric and embedded target boundary points, which are reconstructed employing the method in [3] using $\boldsymbol{R}^{\mathrm{D}}_{\mathrm{R2}}$ and $\boldsymbol{R}^{\mathrm{T}}_{\mathrm{R2}}$ defined in Sect. 2, respectively, before and after waveform compensation. This figure denotes that the FDTD-based waveform compensation enhances the accuracy of inner object imaging.

Finally, for a quantitative analysis of the internal imaging results, a reconstruction accuracy is introduced as

$$\mathrm{err}\left(\tilde{\boldsymbol{q}}_{\mathrm{R1},i}\right) = \min_{\boldsymbol{r}_{\mathrm{true}}} \left\| \hat{\boldsymbol{r}}^{\mathrm{T}}_{\mathrm{R1}}\left(\boldsymbol{q}_{\mathrm{R1},i}\right) - \boldsymbol{r}_{\mathrm{true}} \right\|, \tag{4}$$

where $\boldsymbol{r}_{\mathrm{true}}$ is the location of the true target points, and $\hat{\boldsymbol{r}}^{\mathrm{T}}_{\mathrm{R1}}\left(\tilde{\boldsymbol{q}}_{\mathrm{R1},i}\right)$ denotes an estimated internal target point for each range point $\tilde{\boldsymbol{q}}_{\mathrm{R1},i}$. Figure 7 shows the number of estimated target points for each $\mathrm{err}\left(\tilde{\boldsymbol{q}}_{\mathrm{R1},i}\right)$ before and after waveform compensation. This figure quantitatively demonstrates that the waveform compensation significantly upgrades imaging accuracy, where the mean error for embedded target boundary estimation before and after waveform compensations are $1.98 \times 10^{-2}\lambda$ and $0.97 \times 10^{-2}\lambda$, respectively.

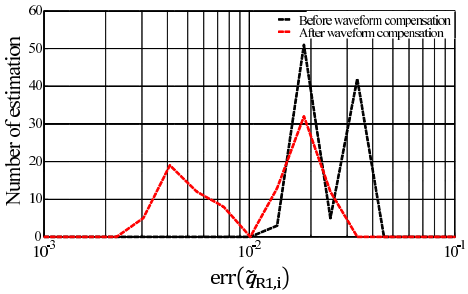

Fig. 7 Histogram for estimation error of inner target points before and after waveform compensation.

5. Conclusion

This paper investigated the existing method in [7] with experimental data, where a creeping wave suppression scheme was introduced by exploiting a unique feature of the RPM and Envelope methods. In the experimental validation, this method simultaneously achieved highly accurate dielectric constant estimation and embedded target reconstruction of the order of 1/100 of the wavelength scale. However, it should be noted that this experimental setup assumes considerably ideal situation, that both outer and inner cylinder objects with exact circle cross section are located at the center point of the rotating, namely, symmetric object shape and scanning trajectory. In the case of asymmetry object shape such as investigated in [7], the creeping waves propagating the right and left side of outer boundary are separately observed at the receiving antenna. While the two propagation paths can be estimated by our proposed method, there is the possibility that the transmissive signal would not be clearly extracted, compared with the symmetric case. In addition, the difficulty for suppressing the creeping wave becomes more severe, when the dielectric constant and the size of outer dielectric medium becomes small, because the difference of time delay between creeping and transmissive waves becomes also small, that causes the interference of these two components. Such investigations for more elaborate target shape or severe case in the experiment should be assessed in our future work to assure the effectiveness of our proposed method.

References

[1] P. Kosmas, and C.M. Rappaport, "A Matched-Filter FDTD-Based Time Reversal Approach for Microwave Breast Cancer Detection," IEEE Trans. Antennas Propag., vol.54, no.4, pp.1257–1264, April 2006.

[2] X. Li, E.J. Bond, B.D. Van Veen, and S.C. Hagness, "An overview of ultrawideband microwave imaging via space-time beamforming for early-stage breast cancer detection," IEEE Trans. Antennas Propag., vol.47, no.1, pp.19–34, Feb. 2005.

[3] K. Akune, S. Kidera, and T. Kirimoto, "Accurate and Nonparametric Imaging Algorithm for Targets Buried in Dielectric Medium for UWB Radars," IEICE Trans. Electronics, vol.E95-C, no.8, pp.1389–1398, Aug. 2012.

[4] S. Kidera, T. Sakamoto, and T. Sato, "Accurate UWB Radar Three-

Dimensional Imaging Algorithm for a Complex Boundary Without Range Point Connections," IEEE Trans Geosci & Remote Sens., vol.48, no.4, pp.1993–2004, April 2010.

[5] A. Franchois and C. Pichot, "Microwave Imaging-Complex Permittivity Reconstruction with a Levenberg-Marquardt Method," IEEE Trans. Antennas Propag., vol.45, no.2, pp.203–215, Feb. 1997.

[6] P. Protiva, J. Mrkvica, and J. Machac, "Estimation of Wall Parameters From Time-Delay-Only Through-Wall Radar Measurements," IEEE Trans. Antennas Propag., vol.59, no.11, pp.4268–4278, Nov. 2011.

[7] R. Souma, S. Kidera, and T. Kirimoto, "Accurate Permittivity Estimation Method with Iterative Waveform Correction for UWB Internal Imaging Radar," IEICE Trans. Electron., vol.E96-C, no.5, pp.730–737, May 2013.

[8] S. Kidera, T. Sakamoto, and T. Sato, "A Robust and Fast Imaging Algorithm with an Envelope of Circles for UWB Pulse Radars," IEICE Trans. Commun., vol.E90-B, no.7, pp.1801–1809, April 2007.

[9] T. Ida, T. Ishihara, and K. Goto, "Frequency-domain and time-domain novel uniform asymptotic solutions for scattered fields by an impedance cylinder and a dielectric cylinder," IEICE Trans. Electron., vol.E88-C, no.11, pp.2124–2135, Nov. 2005.